Imperial College
London

Platform for Microrobot Navigation

Nafiseh Vahabi

''A thesis submitted in partial fulfilment of the
requirements for the degree of MRes in
Medical Robotics and Image Guided Intervention
and for the Diploma of Imperial College''

Imperial College London

April 25, 2014

Project supervisors: Dr. Henry lp, Dr. Vincenzo Curto
and Professor Guang-Zhong Yang

Acknowledgements

I would like to thasnks to

Contents

List of Figures

List of Tables

Abstract

Structures and functions of microorganisms were made them suitable reference to design microrobots. Flagellar propulsion of microorganism such as E.coli is used as an efficient approach for modelling micro swimmers locomotion method in low Reynolds number regime. Microrobots were demonstrated precise and controllable movements under low strength magnetic field. A system with a size of bacteria, capable to swim in viscous fluid in a controllable manner was satisfied basic principles for performing delicate tasks such as targeted drug delivery in medical application. Furthermore microrobots were advantaged from fabrications technology to make them biocompatible. We review a range of bio mimetic microrobots and their fabrication methods and reproduce helical micro swimmers by analysing their mathematical propulsion methods. The definitive microrobots designs were simulated and printed by Nanoscribe technology. Finally,

1   Introduction

The potential use of microrobots in medical applications such as minimally invasive surgery has attracted scientists to work on designing microrobots [1]. research into swimming micro-robots showed two primary difficulties are the power source and finding suitable locomotion methods, as there are many cells, proteins and fibres in biofluids that prevent the motion of the microrobots [9].

Artificial bacteria flagella is most popular microrobots were inspired by nature [12]. They have helical shape, are composed of magnetic material and are capable to mimick three dimentional motion of the bacteria in a high viscous fluid.

Magnetically actuated helical micromachines can be used in a variety of biomedical applications such as cell characterisation, targeted drug delivery and in vivo diagnosis [8]. However, the issue of biocompatibility and the marterial used to make a microrobot needs to be considered carefully for in vivo application[12]. Section 2.2 presents a prief histery of fabrication techniques and section 3.3 describes the fabrication method is applyed in this study. In addition, the extremely small size of the microrobots and the complex biofluid environment make the design aspect very challenging.

The design of microrobots depends on their application and the desired task. An overview of the different microrobot designs, their structures and fabrication methods are discussed in the chapter 2, literature review, .

For the purpose of this project different proposed structures of microrobots were studied and analysed. This will enable helical microswimmers to be reproduced. Once reproduced, the aim of this project will be to compare the efficiency, power, motion velocity and cost-efficiency of various microrobot designs for mass production of the microswimmers. The fabrication of microswimmers will be by Nanoscribe facility using 3D laser lithography. After the microrobots are produced their characteristic will be analysed under the scanning electron microscope in order to identify further improvements in microrobot design.

1.1   Problem

1.2   Previous work

2 Literature review

2.1 Bioinspired microrobots

One of the most challenging aspects of designing a robot on a very small scale such as a nanorobot is simplicity. The reason is, integration will become unfeasible on that scale if the design is complex. Hence the development of the nanorobot or even microrobot should be based on the essential functionality, avoiding any unnecessary components [2]. By learning from nature and mimicking the structure of live organisms, the successful scientific applications were created [13]. In the following section a few examples of microrobots that were imitated from nature will describe.

Reynolds number   To understand how micro organisms swim in a fluidic environment, it is essential to study their propulsion mechanism. In the fluidic regime the Reynold number (Re) has a substantial effect on a microdevice locomotion [8]. The Reynolds number describes the ratio of the inertial forces versus viscous forces according the following formula;

$$Re = \frac{ULρ}{μ} \tag{2.1}$$

Where U is velocity, L is characteristic length, $ρ$ is the density and $μ$ is viscosity of the fluid.

2.1.1 Flagella style microrobots

Helical flagella and cilia are two well-known microswimers in nature that have had their functionality employed for motion generation in artificial microrobots (Figure 2.1) [2].

In 2007, Bell [2] presented the first artificial bacteria flagellum microrobots and then Zhang characterised them in 2009 [2]. This microrobot was formed of two components; a rigid helical tail and a soft magnetic metal head. The head diameter was $2.8μm$ and its length was $30 - 100μm$. Since then, other scientists proposed a slightly different design structure, that all have the rigid helical tail structure. However, in some cases the magnetic materials is used in the device tail rather than the head [2].

The helical rotation of flagella and the travelling wave beat of cilia are two non-reciprocal propulsion mechanisms in microorganisms. Mimicking a rotating flagellum at low Reynolds number to generate an adequate
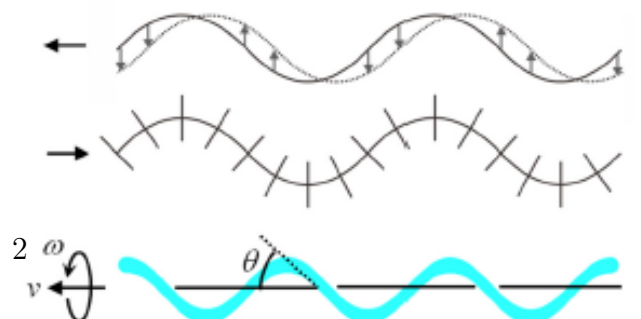
Figure 2.1: The illustration of both flagellum and cilia shapes and microdevices mimicked the flagellum and cilia structures. [9].

torque to overpower the high viscous drag requires two main elements; a rotary motor and a power source [13]. An electromagnetic rotary motor can be used in designing a helical flagella style microrobot that requires a considerable current. However piezoelectric rotary motors are an alternative option that are appropriate for miniaturisation but nec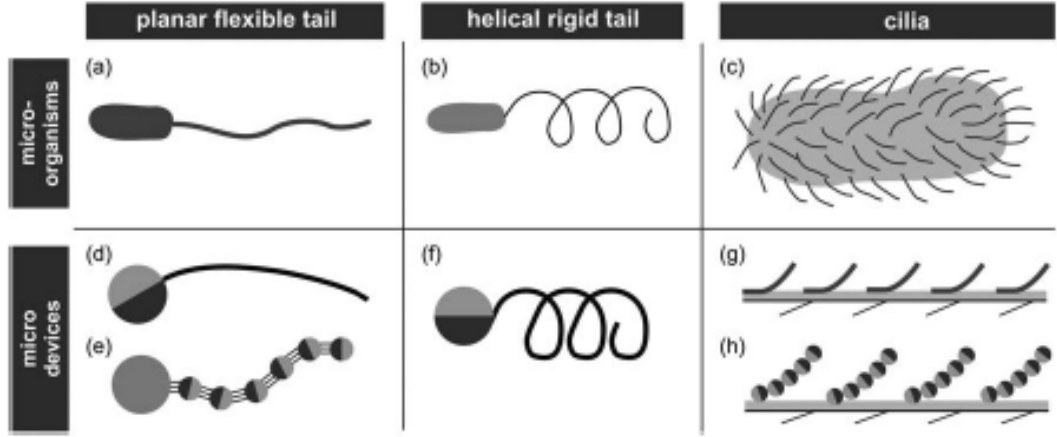essitate high input voltage. Hence, designing a microrobot with a combination of an onboard power source and a motor is a challenging task [13].

Another design of microswimmers was inspired by the function of magtigonemes in nature [16]. A smooth flagellum moves against the direction of the propagation of the flagella wave. However, the flagellum covered by magtigoneme propels in the same direction as the flagellum wave (Figure 2.2). Mimicking the structure of flagellum and using 3D lithography and electron beam evaporation formed the fabrication method in these microswimmers. The anisotropic viscous drag on the flagella is an important fact for locomotion in low Reynolds number fluid. Flagella movement in the opposite direction of the flagella wave is because the viscous drag coefficient perpendicular to the flagella is greater than the viscous drag coefficient parallel to the flagella [16].

The rotating field, i.e. rotational frequency, field strength and angles that defined the rotational axis can be controlled by the current in the external coil. The helical microrobots rotate synchronously with the rotation of the magnetic field and move forward and backward accordingly [16]. The displacement of the microswimmer along the rotational axis can be measured and the result used to calculate the average velocity of the swimmers. There is a linear relationship between an input field frequency and swimming speed. According to their result [16], a propulsive force generated by the mastigoneme is in opposite direction of the force generated by the main helical filament. However, this velocity is only valid if the external force is zero. The proposed design [16] is rigid and an external stimulus may be used to regulate the swimming speed and direction if the swimmer can fold and unfold their structure.
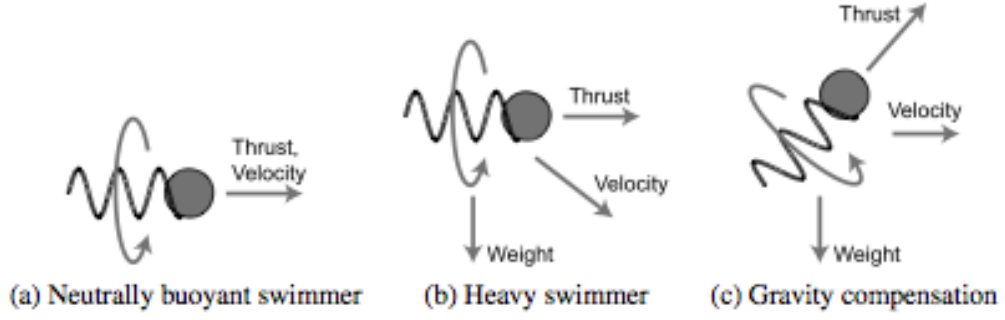
Figure 2.4: The effect of the gravity on the microrobot motion direction and gravity compensation [5].

There are three common shapes of microrobots based on the rotary action; a helix, a screw and a twisted ribbon shape around its axis (Figure 2.3). For the purpose of drilling into solid matter such as biological tissue the screw and helix design would be more appropriate. The rotational motion of helical micro swimmers is one of the most effective propulsion methods in the low Reynolds number scenarios because it leads to translational motion. Microrobots with the microspheres structure perform similarly to the helical swimmers and are capable of swimming in the flowing liquid within the microfluidic channel [3].

There are two main factors that affect the movements of the microrobot in the external magnetic field; low coercivity and high saturation magnetization. Also, the motion of the microrobot is related to its size given the same magnetic field strength and as such, by increasing the size of the microrobot with the inflexible magnetic material volume, the velocity will decrease [3]. The surface friction and the drag forces are two resistive forces that impede the microrobot's motion. Hence, the input magnetic force must be sufficient to overcome these forces for microrobot manipulation. Furthermore, the weight of the microrobot requires gravity compensation in the z-direction by the magnetic field. The navigation methodology should compensate for gravity to avoid sinking and enable velocity to be controlled wirelessly. Mahoney et al. described an algorithm for helical microswimmers velocity control plus gravity compensation. In the proposed model the correct pitch angel and rotation speed is calculated to achieve the commanded velocity (Figure 2.4).

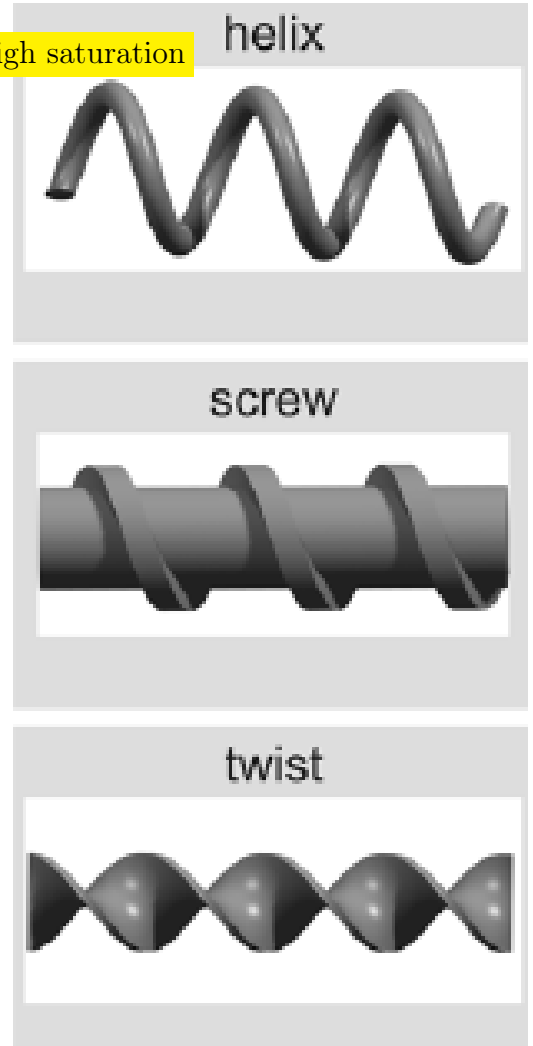The mathematic model below describes the

Figure 2.3: Three design of helical microswimmers. [8].

4

microrobot translational movement;

$$\overrightarrow{F_m} + \overrightarrow{F_r} - \overrightarrow{F_g} = M(\overrightarrow{dv}/dt) \qquad (2.2)$$

Where F_m, F_r and F_g are a magnetic force, overall resistive force and gravitational force respectively. M is a mass and v is a translational velocity of the microrobot [3].

A magnetic field can be used for controlling teams of microrobots as well as a single one. Kim et al. proposed a method that used a combination of two magnetic materials to attain on/off magnetization of each microrobot. The overall control of the group of microrobots was achieved by managing the magnetization state of each microrobot. In addition, a second technique has been developed for three-dimensional motion of the team of microrobots in a fluidic environment. In the latter method, each microrobot is designed in such a way that it uniquely responds to the input magnetic field. Therefore, several microrobots can provide feedback position control in 3D system [3]. An untethered spherical magnetic micromanipulator creates a locally induced rotational fluid flow gradient. The created rotational flow propels micro-objects in the flow area. A team of microrobots could perform a complex task in micro-transport and micro-assembly [3].

In another study [17], a helical microrobot was designed to swim in a low Reynolds number. Two designs are selected to run the experiment; the first one is a bare helical structure and the second one is the helical shape with the microholder attached at the end. Both designs will generate the corkscrew motion in a fluid environment when the magnetic filed is about few mili Tesla. The second design (device with the microholder) is capable of transporting a microobject accurately to the target [17]. size and weight of the object

In Tottori et al.'s study eight designs of microrobots were proposed and tested. The uniform static magnetic field was used to explore the magnetic shape anisotropy and the magnetic actuation was monitored in the rotating magnetic field. In the static magnetic field the set of microrobots had helical angles θ ranging from 45° to 70° when suspended in the deionised water.

This showed (Figure 2.5) that a smaller helix angle θ results in a less misalignment angle α because microrobots longest axes will be aligned to the direction of the external magnetic field. However in helical microrobot with larger helix angles (θ), the magnetization direction would change to the radial axes of the helix [17]. In the rotating magnetic field, the micro helical swimmer exhibits different behaviours depending on the strength of the applied frequency in the fixed magnetic field. At low frequencies the micro helix oscillated
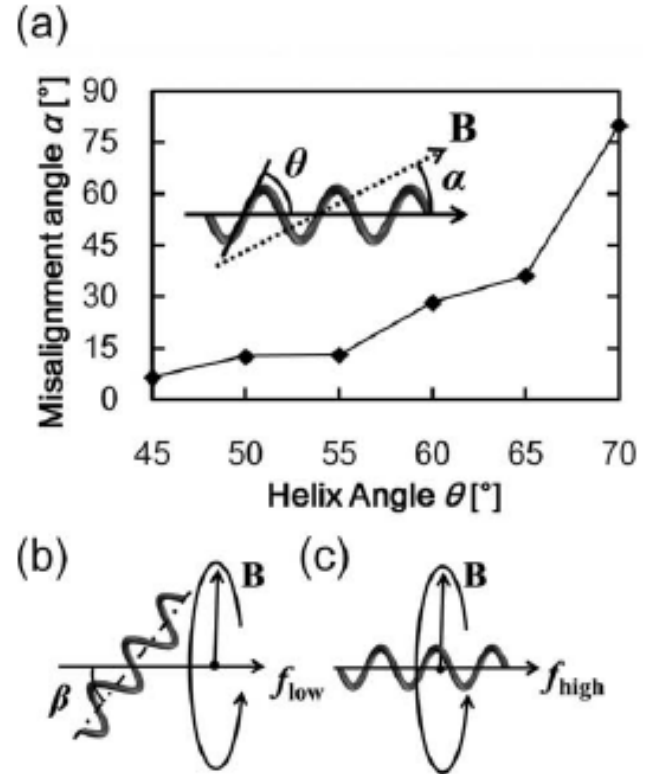

Figure 2.5: (a) The misalignment of helical angle α with differnt helix angle (b) the oscillation behaviour of the microswimmer with the high and low frequencies [17].

5

around the helical axes, however the oscillating behaviour changed to the corkscrew motion after increasing the applied frequency in the magnetic field. This is similar to characteristics of microrobots with an incorporated microholder [17].

The velocity of helical micro swimmers depends on their size and shape. A linear relationship was observed between the input frequencies and swimming velocity of the micro swimmers. The outcome of the comparison between three microhelixs with the same helix angles showed that the microhelix with the greatest diameter has the highest speed, in accordance with the following formula;

$$U = \frac{(C_n - C_1)\sin\theta\cos\theta}{2(C_n\sin^2\theta + C_1\cos^2\theta)}(d\varpi) \qquad (2.3)$$

Where C_n is a drag coefficient perpendicular to the filament and C_1 is a drag coefficient parallel to the filament. ϖ is the rotational frequency and d is the rotational diameter of the helix [17].

The important role of helix angle in the magnetization structure of helical micro swimmers was confirmed by Peyer et al. [7], who used direct laser writing (DLW) as a fabrication method but applied (DLW) on a magnetic polymer composite (MPC). The MPC are non-cytotoxic and showed super paramagnetic characteristic because magnetic material was already included in the polymer.

The relationship between the torque T, the drag force F, the object's velocity ν and rotational speed ω is linear and modelled by 6×6 resistant matrix as below;

$$\begin{bmatrix} F \\ T \end{bmatrix} = \begin{bmatrix} A & B \\ C & D \end{bmatrix} \begin{bmatrix} \nu \\ \omega \end{bmatrix}$$

Where A, B and D are matrices 3x3 and only depend on the object's geometry and fluid velocity. In the study performed by Purcell [10] has been proved matrices B and C are equal ($B = C$) for a typical flagellum. There are few methods in use to model the resistance matrices and low Reynolds flow such as the method of regularized stokeslets, the boundary element method and the method of fundamental solution . In designing a microrobot the main parameters required to concentrate on are the helicity angle ψ, the helix radius R, the pitch p and the filament radius r as illustrated in Figure 2.6 part (c). The details of above methods will discuss in section 4.1 (Mathematical model).

Magnetic actuated microrobot is divided into two categories; torque driven microrobot and force driven microrobots. The micro robot using the torque-driven method is more favourable than the force-driven method because their rotation is based on applying torque rather than a force to pull the device [7].

Another approach for powering a micro robot is using the catalytic conversion of chemical energy into mechanical energy (Figure 2.7). In this method, the catalyst accelerates the consumption
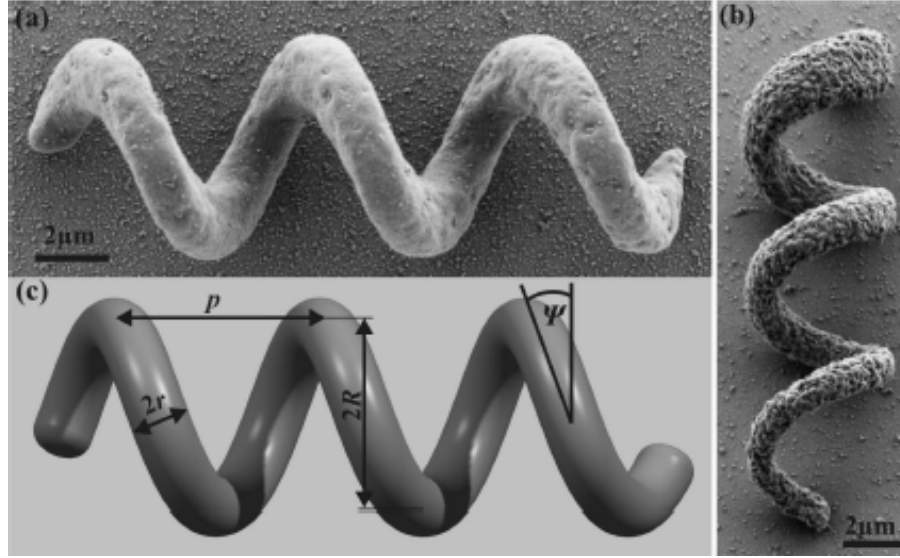
Figure 2.6: The prototype of microhelical device. (a) Scanning electron microscopic image of the micro polymer composite with the 2 vol.% nanoparticle fill factor and (b) 4 vol.% of nanoparticle fill factor. (c) The CAD model shows all the parameters required for the microhelical design [7].

of hydrogen peroxide and helps the self-propulsion of micro robot to pump the fluid to transport cells and colloidal particles [18].

The catalytic tube is fabricated with a sub micrometer diameter. This technique is not applicable for the minimally invasive surgery (MIS) yet because the catalytic material used in the fabrication process of nanotubes is toxic. Hence, biocompatible fuel is required to be developed in order to apply this technique in a live cell environment [18].

Alternatively, the micro driller can be powered and controlled by using an external magnetic field such that changes in the frequency of the rotating magnetic field switch the rotational orientation of the micro tool from the horizontal position to the vertical one. The vertical orientation of the rolled up microtube and its sharp helical design makes the device suitable for drilling into biological tissue. In addition, the micro driller can be used for targeted drug delivery in MIS [18].

2.1.2 Plant-based microrobots

The helical microstructures are not limited to having flagellum-like structures and microbots with general cilia-like feature have been designed. Gao et al. observed the helical microstructures that imitates spiral water-conducting vessels of different plants.
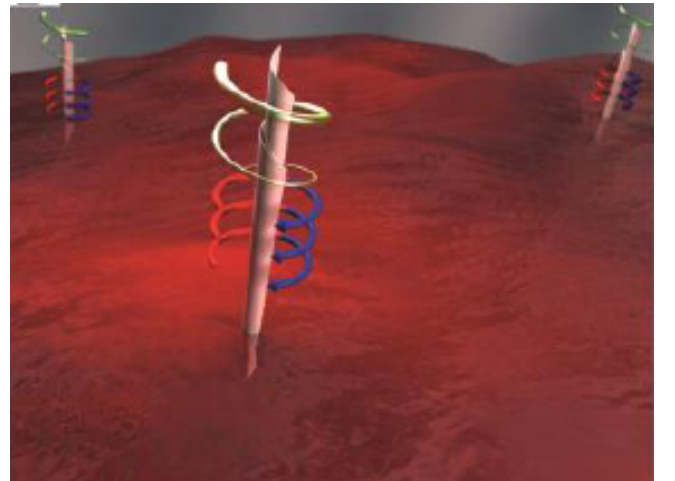

Figure 2.7: Demonstrating the drilling motion of the nanotubes under rotating magnetic field [18].
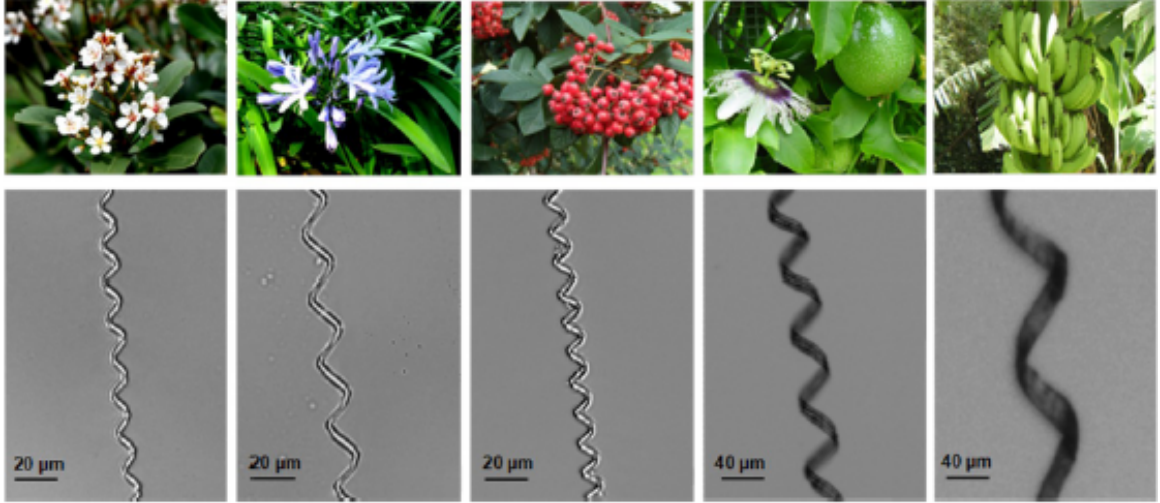
7

Figure 2.8: The shape of the Xylem in differnt plants . [5].

In order to obtain unstretched spiral vessel
several plants were collected and their leaves were macerated and washed with pure water.
Tweezers were used to uncover compressed spiral vessels in the planar networks. Leaves were
gently scored and two segments were pulled apart to a permanent length to stretch the spiral
vessels. These spiral vessel were kept in a glass slides and covered with a thin layer ($20nm$) of
titanium and nickel ($80nm$) using an E-beam evaporator [5]. The helical vessels were coated
in nail polish and baked for 2 minutes to impound the helix and protect the structure. The
final product is a photoresist film on glass that was cut into required lengths.

The fabrication process involves coating isolated spiral xylem vessel plant fibres within a (Fig-
ure 2.6) thin magnetic layer. Xylem tissue transports the plant's required food such as water
and other nutrition from the root to the leaves using capillary action [5]. Use of plant material
in this method enables simple three-dimensional microswimmers fabrication and biocompatibil-
ity. In addition, the magnetic cover helps to ensure accurate directional control and high-speed
propulsion. Therefore the fabrication processes were extremely simplified as the main compo-
nent of the helical microswimmers is from nature and more than a million individual micro
helicals can be made from a very small section of the plant stalk [5].

Using mechanical stretching can control geometric variables of the helical vessels such as the
pitch and helix angle and hence plenty of helical microswimmers can be reproduced. The
final shape of the helical microswimmer is determined mainly by the initial diameter of the
unstretched spiral vessel. The process of stretching helical plant structure was performed via
plastic deformation so that the number of helical turns are constant and tensile stretching of
the plant fibre stretching is negligible [5].

The method used for precise propulsion con-
trol and characterising the locomotion be-
haviour of the plant-based microswimmers is
similar to the method applied in Gao et al.
study.

According to Gao et al. [2] experiment, the
plant-based microswimmers exhibited high
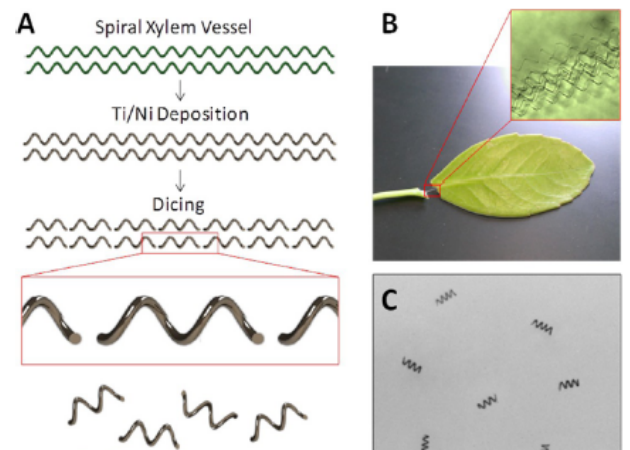
speed movement (85 μm) in raw biological medium such as pure human serum under the rotating magnetic field. However, their swimming speed in pure water (90 μm) was slightly higher than human serum. Hence, an increased velocity of the biological fluid has a minor effect on the plant-driven microswimmers, which is an important advantage of this microdevice over the common microrobots

2.1.3   Jellyfish style microrobots

For the purpose of this project different proposed structures of microrobots were studied and analysed. This will enable helical microswimmers to be reproduced. Once reproduced, the aim of this project will be to compare the efficiency, power, motion velocity and cost-efficiency of various microrobot designs for mass production of the microswimmers. The fabrication of microswimmers will be by Nanoscribe facility using 3D laser lithography. After the microrobots are produced their characteristic will be analysed under the scanning electron microscope in order to identify further improvements in microrobot design.

2.2   Fabrication methods

Historically, the fabrication of the microrobot was the main problem that recent fabrication methods offer a feasible solution [2]. In 2007, the first artificial bacteria flagella was fabricated based on thin-film deposition and self-scrolling methods [12]. In this method . They used In-GaAs/GaAs bilayer for fabricating helical tail and Ni for actuation microrobot's head. The similar fabrication method employed by Zhang in 2009 with the addition of a Cr layer between the microrobots' tail and its head [12]. An improved adhesion of microrobot was the result of adding Cr layer.

3D laser direct writing (DLW) and electron beam decomposition are methods used since then. A typical fabrication process consists of two stages. Initially the core structure of the artificial helical microswimmer is printed using 3D lithography and then electron beam evaporation is used for ferromagnetic thin film coating [16]. Performance of each microswimmer (with different design) can be imaged by the scanning electron microscope (SEM). After the fabrication process is completed, the next step is to release the structure into deionised water using the tungsten probe. The tank with deionised water is installed in the middle of the three-axis Helmholtz setup.

To improve biocompatibility for in-vivo applications, the microrobot can be covered with a thin layer of titanium. In addition, the microrobot's structure was layered with nickel for the purpose of magnetic actuation.

Qiu et al. [11] reported a successful application of helical microrobots for drug delivery were

known as "smart" drug carriers. They used DLW for the fabrication method which was consisted of three steps as shown in the Figure 2.10.

The smart drug carriers were coated in a layer of temperature-sensitive liposomes which is composed of a lipid bilayer and was proposed for cancer therapy in local hyperthermia treatments [11]. The main component of temperature-sensitive liposomes is Dipalmi- toylphosphatidylcholine (DPPC) which transforms from solid to liquid gel at the $41°C$ and released encapsulated drugs.

Qiu et al. [12] were used commercially available material such as ORMOCOMP for fabrication of helical microrobots in their recent experiment. ORMOCOMP is a biocompatible photoresist which can improve the potential use of microrobots for in vivo applications becuase it supports viability, cell proliferation and normal morphology of various cell lines. For the purpose of magnetic microrobot actuation, soft magnetic material such as Fe, Ni and Co are commonly used in microscale structures. The main reason is their biocompatibility with surface decomposition methods, however Ni and Co are cytotoxic and pure iron can be biodegradable [12]. ORMOCOMP helical swimmers were coated onto a thin layer of Fe $(25nm)$ using electron beam decomposition.
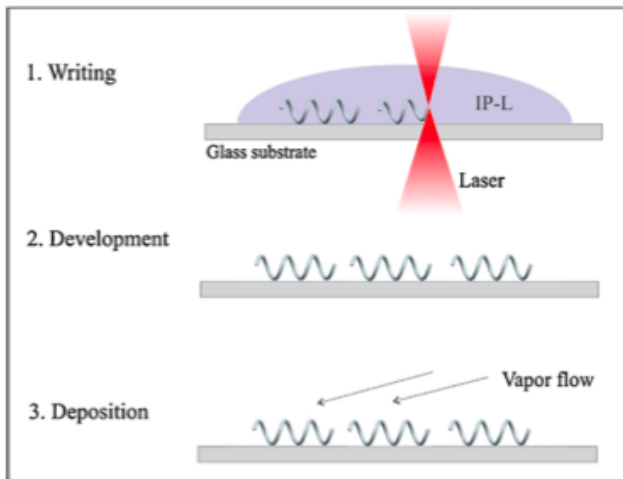

Figure 2.10: DLW steps. step 1 is writting helical microrobots, in step 2 microrobots were developed in isopropyl alcohol and step 3 is coating them by a layer of Ni and Ti. [11].
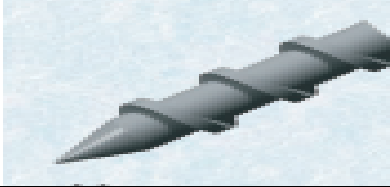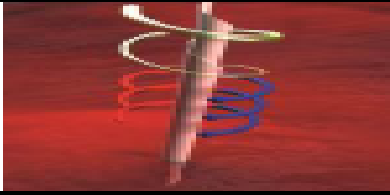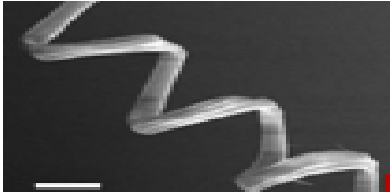
Microrobot Image	Type	Fabrication Method	Citation
	• Helical Screw Shape	• Direct Laser Writting (DLW) • Two-photon Polymerization	• [8]
	• Flagella Shape	• Direct Laser Writting (DLW) • Two-photon Polymerization	• [9]
	• Nanotube	• Molecular Beam Epitaxy (MBE)	• [18]
	• Plant-based	• Macerating Plant's Leaves • Seperating Spiral Vessels • Stretching spiral Vessels • Coating with Titanium	• [2]
	• Jellyfish	• The EMA coil system	• [4]

Table 2.1: Different types of microrobots and their fabrication method.

3 Methods

3.1 Microrobot structure

One of the main requirement of the magnetic microrobot is using magnetic material in their structure to perform actuation task [12].

3.2 Microrobot design

The lenght of the microrobots used by Qiu et al. [12] was $15.7\mu m$ and its diameter was $5.3\mu m$.

Author	Shape	Length	Pitch	Pitch-angle	Radius	Filament-radius	Speed
Arcene	Dense	1000	1000	1000	1000	1000	1000
Dexter	Sparse	20000	1000	1000	1000	1000	1000
Dorothea	Sparse	10000	1000	1000	1000	1000	1000

Table 3.1: Microrobot's design comparisons

3.3 Microrobot fabrication

3.3.1

4 Simulation

Analysing fluid dynamic phenomena on microorganism is a fundamental approach to model microorganism locomotion [15].

A helical bacterial flagellum can be uesed as a reference to model a helical microrobot. The essential parameters to model a helix are, helix length (L), pitch (λ), pitch angle (θ), radius (R), filament radius (a) and contour length ($\Lambda = L/\cos\theta$). Figure 4.1 shows the helix parameters evidently [14]. The flagella parameters were measured for several species of bacteria and its result showed the helical pitch is typically ranging between $2R$ and $11R$, ($2R < \lambda < 11R$). Also the helix length (L) varies from 3λ to 11λ, ($3\lambda < L < 11\lambda$).
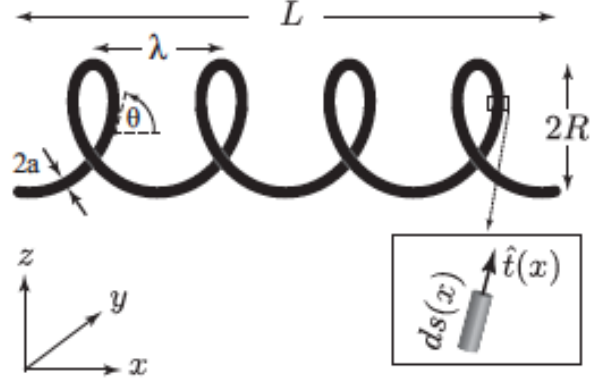
Figure 4.1: The essential helix parameters to design a helical microrobot [14].

4.1 Mathematical model

The flagella rotation at low Reynolds number exerts an axial thrust (F) and torque (T) related to the rotation rate (ω) and flagellum axial velocity (ν). At the same time, fluids was exerted the force ($-F$) and the torque ($-T$) on the swimming microrobots [10]. The fluid dynamic govern by the Stokes equations (4.21) in the low Reynolds regime;

$$-\nabla p + \eta \nabla^2 \nu = 0 \tag{4.1}$$

Where η and p are fluid dynamic velocity and pressure respectively. Therefore thrust (F) and torque (T) are linearly related to the ν and ω as there are no derivation of time in the equations 4.21. Thses linear relationship can be defined as follow;

$$F = A\nu + B\omega \tag{4.2}$$

$$T = C\nu + D\omega \tag{4.3}$$

Therfore, a matrix $\left(\begin{smallmatrix} A & B \\ C & D \end{smallmatrix} \right)$ defined as propulsion matrix the model to explain the flagellar swimming motion described by following equation [14] as mentioned in the literature review earlier;

$$\begin{bmatrix} F \\ T \end{bmatrix} = \begin{bmatrix} A & B \\ C & D \end{bmatrix} \begin{bmatrix} \nu \\ \omega \end{bmatrix}$$

The elements in the symetric 2×2 matrix (propulsive matrix) in the above equation only depends on flagellum geometry. The propulsive matrix elements can be computed by three methods called; resistive force theory, slender body theory and regularized Stokeslet theory in sections 4.1.1, 4.1.3 and 4.1.2 respectively.

4.1.1   Resistive force theory
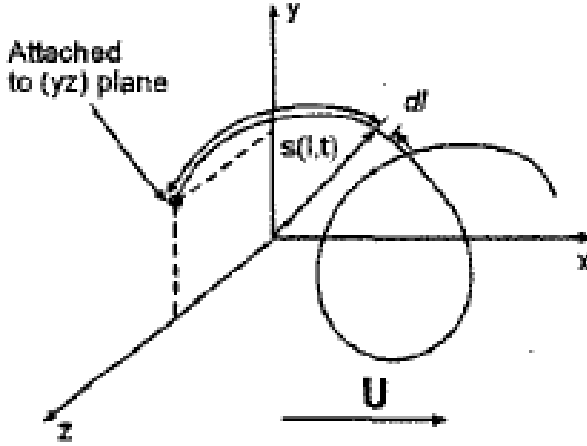
Figure 4.2: A motion of an arbitary filament [1].

The swimming velocity and efficiency of the microrobot can be predicted by Resistive force theory (RFT) [10]. The force exerted on the fluid by micro swimmer were calculated initially and the micro swimmer will have a net movement if the force is not zero [6]. Furthermore, the swimming velocity will decrease if the helical body attached to the innert head. Figure 4.2 shows an arbitary filament motion which is defined by $s(l,t)$. A direction of the helix velocity (U) is along x-axis and its rotation is symetric about the x-axis. The follow-

Figure 4.3:   [1].

ing assumption has been made in order to use the RFT. The geometry of the helix is on the yz-plane and it always attached to the robot body (can be a sphere). The filament motion is periodic and filament length is constant at all the time. Acceleration can be neglected as the system is in the low Re number fluid. Hence, the equations 4.17 and 4.18 will describe the force balance and the moment balance in the x-axis direction. The thrust and torque will be determined by integrating over the first term of the force balance and moment balance equations (4.17 and 4.18) respectively [1].

$$\frac{1}{\Delta T} \int_0^{\Delta T} \int_0^L f_x(l,t) \, \mathrm{d}l \, \mathrm{d}t + C_D U = 0 \tag{4.4}$$

14

$$\frac{1}{\Delta T} \int_0^{\Delta T} \int_0^L [\mathbf{r} \times \mathbf{f}(l, t)].\mathbf{e}_x \, \mathrm{d}l \, \mathrm{d}t + C_{D\Omega}\Omega = 0 \tag{4.5}$$

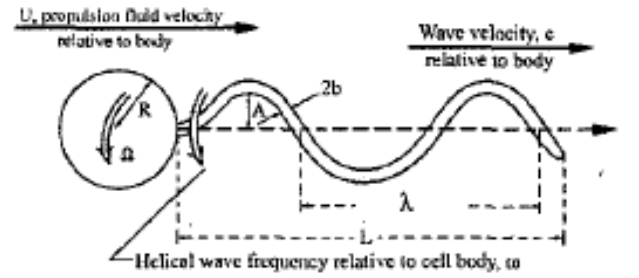Where ΔT is the time filament motion repeats and integration is taken over the whole lenght (L) of the helix.

In order to solve the integration problem, the force (f) is required to be defined. Therefore, a new coordination system was introduced and the force vector was defined as a composition of force per unit length in the normal and tangent directions. Two identical motions are considered for the swmming microrobots are; rotating and translating (assumed in the x-axis direction). Hence, the force balance and moment balance equations are simplified as following;

$$N f_x L + C_D U = 0 \tag{4.6}$$

$$N f_y A L + C_{D\Omega}\Omega = 0 \tag{4.7}$$

Where N and A are number of filaments and helical amplitude of filaments respectively. Also f_x and f_y shows the components of the force vector along x and y directions. In addition, C_D and $C_{D\Omega}$ were computed by equations 4.8 and 4.9 where R is redius of the helix and μ is fluid velocity.

$$C_D = 6\pi\mu R \tag{4.8}$$

$$C_{D\Omega} = 8\pi\mu R^3 \tag{4.9}$$

The f_x and f_y are written as composite of forces in the normal and tangent directions;

$$f_x = f_t \cos\theta - f_n \sin\theta \tag{4.10}$$

$$f_y = f_t \sin\theta + f_n \cos\theta \tag{4.11}$$

$$\tan\theta = \frac{\lambda}{2\pi A} \tag{4.12}$$

$$f_t = -C_t(U\cos\theta - \omega A\sin\theta) \tag{4.13}$$

$$f_n = -C_n(-U\sin\theta - \omega A\cos\theta) \tag{4.14}$$

Where C_t and C_n called resistance coefficients [1];

$$C_t = \frac{2\pi\mu}{\ln(\frac{2\lambda}{b}) - \frac{1}{2}} \tag{4.15}$$

$$C_n = \frac{4\pi\mu}{\ln(\frac{2\lambda}{b}) + \frac{1}{2}} \tag{4.16}$$

Microrobot's swimming speed and rotation rate weer determined by solving the equations 4.13 and 4.14. Therefore, thrust (F), torque (T) and drag (D) on flagellum can be predict by following equations [14];

$$F = (\Omega R)(C_n - C_t)\sin\theta\cos\theta\frac{L}{\cos\theta} \tag{4.17}$$

$$T = (\Omega R^2)(C_n\cos^2\theta + C_t\sin^2\theta)\frac{L}{\cos\theta} \tag{4.18}$$

$$D = U(C_n\sin^2\theta + C_t\cos^2\theta)\frac{L}{\cos\theta} \tag{4.19}$$

Finally, the efficiency of the helical swimmers can be computed as follow;

$$efficiency = \frac{FU}{T\omega} \tag{4.20}$$

Rodenborn et al. [14] demonestrated the failure of resistive force theory to predict thrust and drag in microrobots motion accurately. The reason of the failure was neglecting hydrodynamic interaction between flows induced by different parts of a flagellum. In particular, helical flagellum with smaller pitch (λ) will have smaller separation of filament segments (Figure 4.1). Hence, the hydrodynamic interaction between different parts of a flagellum becomes stronger and in very small pitch $(\lambda \to 0)$ the helix converts to a cylinder which has no thrust $(F = 0)$.

4.1.2 Regularized Stokeslet method

A regularization parameter can be used as a proxy for the body radius to minimise numerical errors in modelling a flagellum as a one dimential filament in a low Reynolds [15]. number fluids. The Regularized Stokeslet method (RSM) is one of the approch to solve the zero Reynolds number linear 'Stokes flow' equations;

$$\left.\begin{array}{l} 0 = -\nabla p + \mu\nabla^2 u + f \\ 0 = \nabla.u \end{array}\right\} \quad \text{Stokes flow equations} \tag{4.21}$$

where u (velocity), p (pressure), μ (kinematic viscosity), and f (force) are measured per unit volume. The singular 'Stokeslet' solution for the equations 4.21 corresponds to the purely

viscous component (point force) of the flow which was determined by moving sphere. The 'Stokeslet' solution for unit force acts in the j-direction and concentrated at ξ, where f is;

$$f(x) = \delta(x - \xi)e_j \tag{4.22}$$

$\delta(x - \xi)$ is called Dirac delta distribution. The velocity in the i-direction driven by this force is defined as follow;

$$S_{ij}(\boldsymbol{x}, \boldsymbol{\xi}) = (\frac{\delta_{ij}}{r} + \frac{r_i r_j}{r^3}) \tag{4.23}$$

Where δ_{ij} denotes Kronecker delta tensor, $r_i = x_i - \xi_i$ and $r^2 = |\boldsymbol{x} - \boldsymbol{\xi}|^2 = r_1^2 + r_2^2 + r_3^2$. The flow concentrates at point $\boldsymbol{\xi}$ by the force $\mathbf{F}$ where $\boldsymbol{f}(\boldsymbol{x}) = \delta(\boldsymbol{x} - \boldsymbol{\xi})\boldsymbol{F}$. The solution is given by finding the velocity $u_i(\boldsymbol{x})$;

$$u_i(x) = (\frac{1}{8\pi\mu})S_{ij}(\boldsymbol{x}, \boldsymbol{\xi})F_j \tag{4.24}$$

The resistive force theory (RFT) and slender body theory (SBT) for modelling of flagellum driven flow were formed on the base of the Stokeslet [15]. These methods solved the three dimentinal flow problem with flexible boundaries without using direct computation for the differential equations. Therefore, the provided solution are extremely efficient in terms of computational costs. The fluid velocity was modeled by the following equation;

$$\mathbf{u}(\mathbf{x}) = (\frac{1}{8\pi\mu}) \int_S \boldsymbol{f}(\boldsymbol{\xi}).\boldsymbol{S}(\boldsymbol{x}, \boldsymbol{\xi}) \, \mathrm{d}S_\xi \tag{4.25}$$

Where S is a collection of lines or surfaces of flagella, $\boldsymbol{f}(\boldsymbol{\xi})$ shows force per unit length or area. $\boldsymbol{f}(\boldsymbol{\xi})dS_\xi$ denotes the force flagella body exerted on the fluid and $-\boldsymbol{f}(\boldsymbol{\xi})dS_\xi$ is the force fluid applies to the body. The flagella is represented by equation 4.25 with the boundary S and parameter $\boldsymbol{\xi}(\boldsymbol{s})$ where $0 < s < 1$ is scaled arclength parameter. However, the flow field at any point $\boldsymbol{x} = \boldsymbol{\xi}(s)$ is sigular and the collection of points on the surface of the filament are required to calculate the force per unit length. The collection of points were replaced on a small distance from the centreline;

$$\mathbf{X}(\mathbf{s_q}) = \boldsymbol{\xi}(s_q) + a(s_q)\boldsymbol{n}(s_q) \tag{4.26}$$

where $a(s_q)$ is a radius of slender body and $\boldsymbol{n}(s_q)$ is a unit normal vector. Point distributions of Stokeslets at any point $x = \boldsymbol{\xi}_q$ and line distribution inside the notional surface of the flagella are both singular. However, surface distributions of Stokeslets do not result in singular velocity but it still require attentive numerical implementations [15]. The 'regularized Stokeslet' introduced an exact solution for the equations 4.27 to overcome these issues. This method used a cut off function (ψ) with a regularization parameter (ϵ) to smooth point forces such that $\int_{R^3} \psi_\epsilon(\boldsymbol{x}) \, \mathrm{d}V_x = 1$.

$$0 = -\boldsymbol{\nabla}p + \mu\nabla^2\boldsymbol{u} + \boldsymbol{f}\psi_\epsilon(\boldsymbol{x} - \boldsymbol{\xi}), \left.\begin{array}{r} \\ \\ \end{array}\right\}$$
$$0 = \boldsymbol{\nabla}.\boldsymbol{u}$$

Stokes flow equations with regularization parameter

(4.27)

In RSM method, with a assumption of $\psi_\epsilon(\boldsymbol{x} - \boldsymbol{\xi}) := 15\epsilon^4/8\pi\mu r_\epsilon^7$ and $r_\epsilon = \sqrt{r^2 + \epsilon^2}$ the regularized Stokeslet velocity tensor measured by the the following:

$$S_{ij}^\epsilon(\boldsymbol{x}, \boldsymbol{\xi}) = \frac{\delta_{ij}(r^2 + 2\epsilon^2) + r_i r_j}{r_\epsilon^3} \tag{4.28}$$

Therefore the boundary for intergal equation (4.29) is defined and the fluid velocity at location x is;

$$\mathbf{u}(\mathbf{x}) = (\frac{1}{8\pi\mu})\int_S \boldsymbol{f}(\boldsymbol{\xi}).\boldsymbol{S}^\epsilon(\boldsymbol{x}, \boldsymbol{\xi})\,\mathrm{d}S_\xi \tag{4.29}$$

Where

4.1.3 Slender body theory

5   Experiments

Fe-ABF and FeTi-ABFs two magnetic fields of strenghts 1mT and 3 mT The test show that forward speed is increasing with increasing input frequency below a critical value called (step-out frequency is the maximum magnetic field frequency that the ABFs can follow synchronously). The step out frequency increases with the strength of the magnetic field. the maximum speed of Fe-ABF was 48.9 $\mu m s^{-1}$ at the field strength of $9mT$ and $72Hz$ [12].

6 Results

7 Discussion

8 Conclusion and future work

References

[1] Jon Edd, Sébastien Payen, Boris Rubinsky, Marshall L Stoller, and Metin Sitti. Biomimetic propulsion for a swimming surgical micro-robot. In *Intelligent Robots and Systems, 2003.(IROS 2003). Proceedings. 2003 IEEE/RSJ International Conference on*, volume 3, pages 2583–2588. IEEE, 2003.

[2] Wei Gao, Xiaomiao Feng, Allen Pei, Christopher R Kane, Ryan Tam, Camille Hennessy, and Joseph Wang. Bioinspired helical microswimmers based on vascular plants. *Nano letters*, 14(1):305–310, 2013.

[3] Sangwon Kim, Famin Qiu, Samhwan Kim, Ali Ghanbari, Cheil Moon, Li Zhang, Bradley J Nelson, and Hongsoo Choi. Fabrication and characterization of magnetic microrobots for three-dimensional cell culture and targeted transportation. *Advanced Materials*, 25(41): 5863–5868, 2013.

[4] Youngho Ko, Sungyoung Na, Youngwoo Lee, Kyoungrae Cha, Seong Young Ko, Jongoh Park, and Sukho Park. A jellyfish-like swimming mini-robot actuated by an electromagnetic actuation system. *Smart Materials and Structures*, 21(5):057001, 2012.

[5] Arthur W Mahoney, John C Sarrazin, Eberhard Bamberg, and Jake J Abbott. Velocity control with gravity compensation for magnetic helical microswimmers. *Advanced Robotics*, 25(8):1007–1028, 2011.

[6] A J Mestel. Biofluids lecture 3: Flagellar swimming, resistive force theory @ONLINE, January 2013. URL `http://www2.imperial.ac.uk/ ajm8/BioFluids/`.

[7] Kathrin E Peyer, Erdem C Siringil, Li Zhang, Marcel Suter, and Bradley J Nelson. Bacteria-inspired magnetic polymer composite microrobots. In *Biomimetic and Biohybrid Systems*, pages 216–227. Springer, 2013.

[8] Kathrin E Peyer, Soichiro Tottori, Famin Qiu, Li Zhang, and Bradley J Nelson. Magnetic helical micromachines. *Chemistry-A European Journal*, 19(1):28–38, 2013.

[9] Kathrin E Peyer, Li Zhang, and Bradley J Nelson. Bio-inspired magnetic swimming microrobots for biomedical applications. *Nanoscale*, 5(4):1259–1272, 2013.

[10] Edward M Purcell. The efficiency of propulsion by a rotating flagellum. *Proceedings of the National Academy of Sciences*, 94(21):11307–11311, 1997.

[11] Famin Qiu, Rami Mhanna, Li Zhang, Yun Ding, Satoshi Fujita, and Bradley J Nelson. Artificial bacterial flagella functionalized with temperature-sensitive liposomes for controlled release. *Sensors and Actuators B: Chemical*, 2014.

[12] Famin Qiu, Li Zhang, Kathrin E Peyer, Marco Casarosa, Alfredo Franco-Obregón, Hongsoo Choi, and Bradley J Nelson. Noncytotoxic artificial bacterial flagella fabricated from biocompatible ormocomp and iron coating. *Journal of Materials Chemistry B*, 2(4):357–362, 2014.

[13] Tian Qiu, John G Gibbs, Debora Schamel, Andrew G Mark, Udit Choudhury, and Peer Fischer. From nanohelices to magnetically actuated microdrills: a universal platform for some of the smallest untethered microrobotic systems for low reynolds number and biological environments.

[14] Bruce Rodenborn, Chih-Hung Chen, Harry L Swinney, Bin Liu, and HP Zhang. Propulsion of microorganisms by a helical flagellum. *Proceedings of the National Academy of Sciences*, 110(5):E338–E347, 2013.

[15] David J Smith. A boundary element regularized stokeslet method applied to cilia-and flagella-driven flow. *Proceedings of the Royal Society A: Mathematical, Physical and Engineering Science*, 465(2112):3605–3626, 2009.

[16] Soichiro Tottori and Bradley J Nelson. Artificial helical microswimmers with mastigoneme-inspired appendages. *Biomicrofluidics*, 7(6):061101, 2013.

[17] Soichiro Tottori, Li Zhang, Famin Qiu, Krzysztof K Krawczyk, Alfredo Franco-Obregón, and Bradley J Nelson. Magnetic helical micromachines: fabrication, controlled swimming, and cargo transport. *Advanced materials*, 24(6):811–816, 2012.

[18] Wang Xi, Alexander A. Solovev, Adithya N. Ananth, David H. Gracias, Samuel Sanchez, and Oliver G. Schmidt. Rolled-up magnetic microdrillers: towards remotely controlled minimally invasive surgery. *Nanoscale*, 5:1294–1297, 2013.